Princeton Plasma Physics Laboratory

PPPL- 4950

PPPL- 4950

Three Dimensional Distortions of the Tokamak Plasma Boundary

I.T. Chapman, M. Becoulet, T. Bird, J. Canik, S. Lazerson, et al.

October 2013

PPPL PRINCETON PLASMA PHYSICS LABORATORY

Prepared for the U.S. Department of Energy under Contract DE-AC02-09CH11466.

Princeton Plasma Physics Laboratory
Report Disclaimers

Full Legal Disclaimer

Trademark Disclaimer

PPPL Report Availability

Princeton Plasma Physics Laboratory:

http://www.pppl.gov/techreports.cfm

Office of Scientific and Technical Information (OSTI):

http://www.osti.gov/bridge

Related Links:

U.S. Department of Energy

Office of Scientific and Technical Information

Fusion Links

Three dimensional distortions of the tokamak plasma boundary: II. Boundary displacements in the presence of resonant magnetic perturbations

IT Chapman[1], M Becoulet[2], T Bird[3], J Canik[4], M Cianciosa[5], WA Cooper[6], T Evans[7], N Ferraro[7], C Fuchs[8], M Gryaznevich[1], Y Gribov[9], C Ham[1], J Hanson[5], G Huijsmans[9], A Kirk[1], S Lazerson[10], Y Liang[11], I Lupelli[1], R Moyer[12], C Nührenberg[3], F Orain[2], D Orlov[12], W Suttrop[8], D Yadykin[13], the ASDEX Upgrade, DIII-D, MAST and NSTX Teams and EFDA-JET contributors*

[1]EURATOM/CCFE Fusion Association, Culham Science Centre, Abingdon, Oxon, OX14 3DB, UK
[2]CEA, IRFM, F-13108 Saint-Paul-lez-Durance, France
[3]Max Planck Institute for Plasma Physics, EURATOM Association, Wendelsteinstr. 1, 17491 Greifswald, Germany
[4]Oak Ridge National Laboratory, Oak Ridge, Tennessee 37831-8071, USA
[5]Auburn University, Physics Department, Auburn, AL 36849, USA
[6]CRPP, Association EURATOM/Confédération Suisse, EPFL, 1015 Lausanne, Switzerland
[7]General Atomics, PO Box 85608, San Diego, CA 92186, USA
[8]Max-Planck-Institut fur Plasmaphysik, EURATOM-Ass D-85748 Garching, Germany
[9]ITER Organisation, Route de Vinon sur Verdon, St-Paul-lez-Durance, France
[10]PPPL, Princeton University, PO Box 451, Princeton, NJ 08543, USA
[11]Forschungszentrum Jülich GmbH, IEF-4, 52425 Jülich, Germany
[12]University of California, San Diego, USA
[13]EURATOM/VR Association, Chalmers University, Gothenburg, Sweden
*See the Appendix of F. Romanelli *et al.*, Fusion Energy 2012 (Proc. 24th Int. Conf. San Diego, 2012) IAEA, (2012)

Abstract.

The three dimensional plasma boundary displacements induced by applied non-axisymmetric magnetic perturbations have been measured in ASDEX Upgrade, DIII-D, JET, MAST and NSTX. The displacements arising from applied resonant magnetic perturbations (RMPs) are measured up to ±5% of the minor radius in present day machines. Good agreement can be found between different experimental measurements and a range of models – be it vacuum field line tracing, ideal three dimensional MHD equilibrium reconstruction, or nonlinear plasma amplification. The agreement of the various experimental measurements with the different predictions from these models is presented, and the regions of applicability of each discussed. The measured displacement of the outboard boundary from various machines is found to correlate approximately linearly with the applied resonant field predicted by vacuum modelling (though it should be emphasised that one should not infer that vacuum modelling accurately predicts the displacement inside the plasma). The RMP-induced displacements foreseen in ITER are expected to lie within the range of those predicted by the different models, meaning less than ±1.75% (±3.5cm) of the minor radius in the H-mode baseline and less than ±2.5% (±5cm) in a 9MA plasma. Whilst a displacement of 7cm peak-to-peak in the baseline scenario is marginally acceptable from both a plasma control and heat loading perspective, it is important that ITER adopts a plasma control system which can account for a three dimensional boundary corrugation to avoid an $n = 0$ correction which would otherwise locally exacerbate the displacement caused by the applied fields.

1. Introduction and Background

When tokamak plasmas operate in a high-confinement regime, the plasma edge is usually susceptible to quasi-periodic instabilities called Edge Localised Modes (ELMs) [1]. These ELMs are understood to be a manifestation of so-called peeling-ballooning instabilities driven by strong pressure gradients and localised current density at the edge of the plasma [2, 3]. ELMs can eject potentially damaging levels of energy and particles from the confined plasma, hence affecting the lifetime of plasma facing components [4]. In order to avoid damage to vessel components in ITER a robust ELM control scheme is required which either suppresses the ELMs completely or, at least, reduces the heat flux per ELM which is incident on the divertor plates [5]. One such control scheme is the application of resonant magnetic perturbations (RMPs), which perturb the magnetic field in the edge transport barrier, or pedestal, region. RMPs have been applied to completely suppress ELMs in DIII-D [6, 7] and KSTAR [8], or to mitigate ELMs – that is to say increase their frequency and reduce their amplitude – in ASDEX Upgrade [9, 10], MAST [11, 12, 13] and JET [14, 15]. Although control of ELMs by applying RMPs clearly involves imposing a non-axisymmetric perturbation to the magnetic field, the plasma is still often treated two dimensionally in equilibrium reconstruction and stability analyses [16, 7, 17, 18, 19, 20].

However, previous results [21, 22, 23, 24, 25, 26, 27, 28] have shown that the application of resonant magnetic perturbations can cause significant non-axisymmetric distortions to the plasma boundary. Such perturbations to the boundary could lead to unacceptable heat loads on the plasma facing components in ITER. The allowable plasma displacement to avoid damage to the first wall has been assessed as 8cm with empirical extrapolation [29] or three-dimensional scrape-off layer transport modelling [30], whilst the boundary must stay within a 4cm envelope of its set-point to achieve good RF coupling [31]. Consequently it is important that we can predict the likely distortions in ITER and prepare methods for the avoidance or control of such boundary displacements.

Past experiments to measure the plasma perturbation when non-axisymmetric perturbation fields are applied have been performed on DIII-D [21, 27, 28], ASDEX Upgrade [22, 23, 24], MAST [25, 26] and JET [25, 32]. In most cases, applied fields from either ex- or in-vessel correction coils had a demonstrable and significant effect on the toroidal periodicity of the plasma edge, deforming the separatrix by a few percent of the minor radius.

Measurements of the displacements caused by applying non-axisymmetric magnetic perturbations in ASDEX Upgrade, DIII-D, JET, MAST and NSTX are presented in section 2. In section 3, these measurements are compared to numerical modelling, either treating the field perturbation using just the vacuum field approximation, including an ideal plasma response, or a nonlinear resistive plasma response. Finally, predictions for the displacements expected in ITER due to externally applied RMPs are made in section 4, before the implications are discussed in section 5.

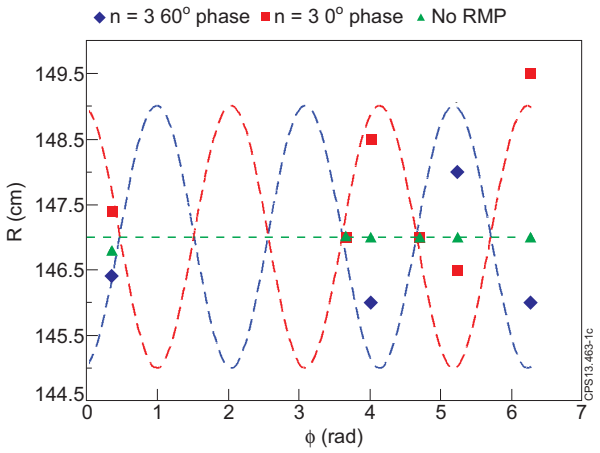

Figure 1. MAST The midplane boundary position as a function of toroidal angle as measured by six different diagnostics with sub-cm radial resolution in MAST plasmas with two phases of an applied $n = 3$ RMP applied. The dashed line is added with $n = 3$ periodicity and arbitrary amplitude to guide the eye.

2. Measurements of displacements due to RMPs in present machines

The effect of applying perturbations with different toroidal mode number has been investigated in MAST double null diverted (DND) plasmas optimised for diagnostic coverage. The primary diagnostics used to measure the radial position of the edge of the plasma are: the linear D_α camera, the phantom colour camera, the charge exchange recombination spectroscopy diagnostic, the RGB camera, a charge-coupled device (CCD) camera, the reflectometer and the Thomson scattering diagnostic, all of which measure the boundary in different toroidal positions. Since there are twelve lower in-vessel coils in MAST, the phase of the $n = 3$ applied field can easily be changed in 30° quanta. In order to maximise the measurable perturbation of the edge of the plasma, two phases of an $n = 3$ RMP were applied with 60° between them. This has the added benefit that the position controller does not significantly correct for the distortion due to the applied RMPs as it is constrained by measurements of the plasma position in a sector experiencing a null in displacement for both phases of applied field. The radial position of the plasma boundary for six different high resolution diagnostics when the two phases of RMPs are applied (compared to a reference plasma in the absence of non-axisymmetric applied fields) is shown in figure 1 [26]. The expected toroidal phase dependence (with arbitrary amplitude) is added to guide the eye. It is clear that not only is there a different dependence of the edge corrugation in the two phases of the applied field, the toroidal variation follows the expected $n = 3$ periodicity symptomatic of the RMP applied. Furthermore, the amplitude of the displacement is found to be in good agreement on a number of different diagnostics and is approximately ±1.5cm, which represents more than ±2.5% of the minor radius [26].

A similar dependence is found when two phases of an $n = 4$ RMP field are applied,

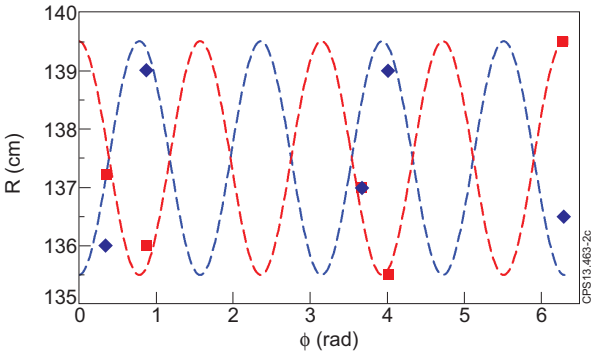

Figure 2. MAST The midplane boundary position as a function of toroidal angle as measured by six different diagnostics with sub-cm radial resolution in MAST plasmas with two phases of an applied $n = 4$ RMP applied. The dashed line is added with $n = 4$ periodicity and arbitrary amplitude to guide the eye.

with figure 2 showing a clear $n = 4$ toroidal periodicity, again with an amplitude of toroidal corrugation of approximately $\pm$1.5cm. In both figures 1 and 2 the position of the outboard midplane when RMPs are not applied is found to be in good agreement adding credence to the toroidal corrugation measured with RMPs.

Measurement of edge displacements have also been made in JET when $n = 2$ RMPs are applied from the set of ex-vessel error field correction coils (EFCCs) [32]. The direct measurements of the plasma boundary displacement are obtained using high resolution Thomson scattering (HRTS) diagnostic by following the time evolution of the edge density profile. The procedure to determine the pedestal position takes into consideration the HRTS instrument function as described in reference [33]. The time evolution of the EFCC current, plasma boundary displacement measured by the HRTS (scaled to have zero displacement before application of the EFCC produced magnetic field) and the radial magnetic flux measured by the coincident flux loop for the shots with different values of the EFCC current are shown in figure 3. The effect of the field produced by EFCC coils on the plasma boundary is clearly seen in the kinetic measurements. Note a rapid transient drop in the EFCC current occurred at $t = 18$s and this reduction in the applied field is manifest as a reduction in the edge distortion, illustrating the dependence of the edge displacement on the applied field strength.

The response of the plasma controller, whilst not studied in detail, is striking. Figure 4 shows the measured displacement in JET when the plasma position feedback uses either the gap between the last closed flux surface and the magnetic loops on the centre column, or the outer gap between the plasma and the low-field side flux loops. It is evident that the plasma control system induces a shift in opposite directions depending upon the position feedback scheme employed. The difference between these two schemes is up to 10cm. This exemplifies the acute need to account for non-axisymmetric displacements in the plasma position control feedback system.

The response of the plasma boundary and separatrix to a 10Hz $n = 2$ oscillating

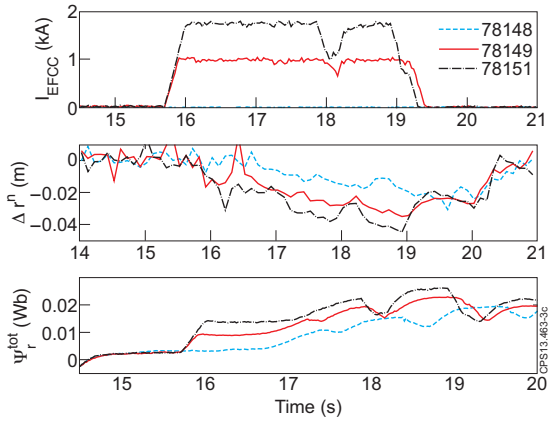

Figure 3. JET The RMP-induced displacement measured by the Thomson scattering diagnostic as a function of time (centre) compared to the coil in the ex-vessel coils in JET (top) and change in the magnetic flux (bottom).

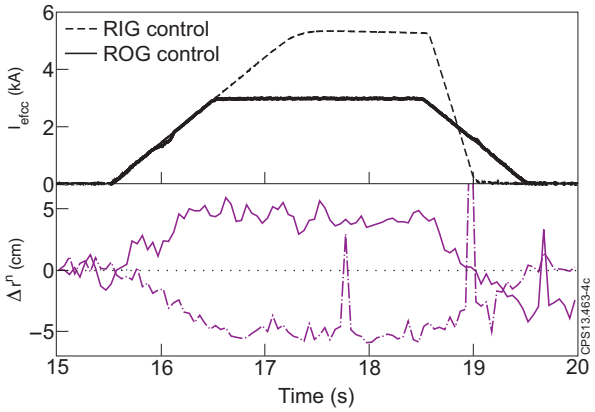

Figure 4. JET The RMP-induced displacement measured by the Thomson scattering diagnostic as a function of time compared to the coil in the ex-vessel coils in JET. The plasma position control is either done on the gap between the plasma boundary and the inner wall (dashed) or the outer wall (solid).

RMP has been studied on DIII-D using active imaging of the Doppler-shifted Balmer D_α emission from high energy injected neutrals (beam emission spectroscopy, BES) [28]. The measurements were obtained in ELMing H-mode discharges with an ITER-similar shape and pedestal collisionality, $\nu_{,e} \sim 0.3$, similar to pedestal conditions predicted for ITER. The internal RMP coils generated an $n = 2$ even parity RMP rotating counter to the plasma current in the toroidal direction at 10 Hz. The temporal evolution of the measured beam emission at an elevation of $Z = 0.1$m is plotted in figure 5 as a function of major radius R. A coherent oscillation is clearly seen in the radius of the steep gradient region of the profile near $R = 2.30$m. In figure 5, the variation in the beam emission at $(R, Z) = (2.27, 0.1)$ is plotted versus time along with the RMP coil current. The beam emission intensity (thick, dashed red line) oscillates coherently and

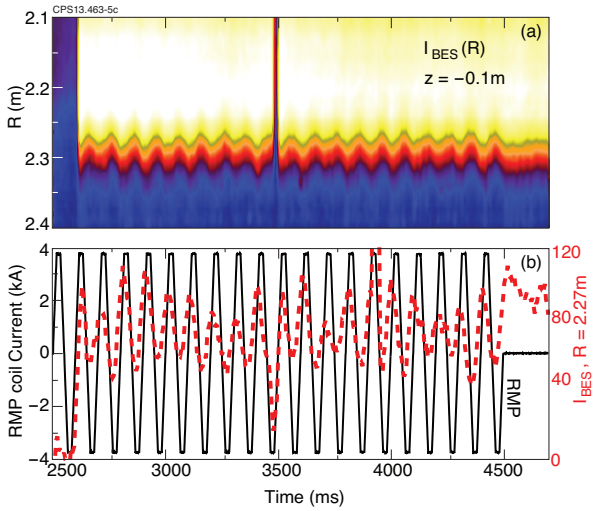

Figure 5. DIII-D (a) Colour contours of the beam emission versus major radius R at an elevation of $z = 0.1$m on the outer midplane of the DIII-D tokamak during the RMP pulse. The rotating $n = 2$ field starts at 2250 ms (before the start of the plot), showing a coherent oscillation in phase with the rotating RMP. (b) Evolution of the rotating $n = 2$ RMP coil current in the upper 150° segment (thin black line), and the measured beam emission intensity (thick red dashed line) at $R = 2.27$m and $z = 0.1$m. The beam emission in the edge is modulated by the rotating $n = 2$ RMP.

is phase locked with the rotating $n = 2$ RMP (thin solid black line), with an amplitude of ±1.5cm, equivalent to ±2.5% of the minor radius [28].

The variation in the electron density profile at an elevation of $Z = 0.05$m on the LFS midplane has also been measured by profile reflectometry in the same DIII-D discharge [28]. There is a clear coherent oscillation in the major radius R of the steep edge gradient region of the profile as the $n = 2$ perturbation is rotated toroidally past the diagnostic which is qualitatively similar to the displacement measured in the beam emission intensity profile. This displacement in the major radius of the steep edge gradient region is on the order of ±1cm, or ±1.7% [28] of the minor radius.

ASDEX Upgrade have also made measurements of the edge displacements when RMPs are applied [22, 24, 23]. A series of identical discharges with 1MA plasma current, a toroidal magnetic field of -2.4 T, fractional Greenwald density of $n_e/n_{GW} \sim 0.64$, 9.7MW additional heating and 1kA in-vessel coil current has been performed, where only the configuration of the in-vessel coils has been varied: 2 discharges with mode number $n = 2$, odd up/down-parity (i.e. opposite polarity of upper and lower coils at the same toroidal position), with zero and 90 degrees toroidal orientation of the magnetic perturbations, and one discharge with n=2, even parity. The density profile measured by the lithium beam diagnostic just before and after the saddle coils have been switched on is shown in figure 6. For an otherwise identical discharge where the configuration of the saddle coils has been rotated by 90° the shift of the perturbed separatrix and correspondingly the shift in the density profile goes in the opposite direction.

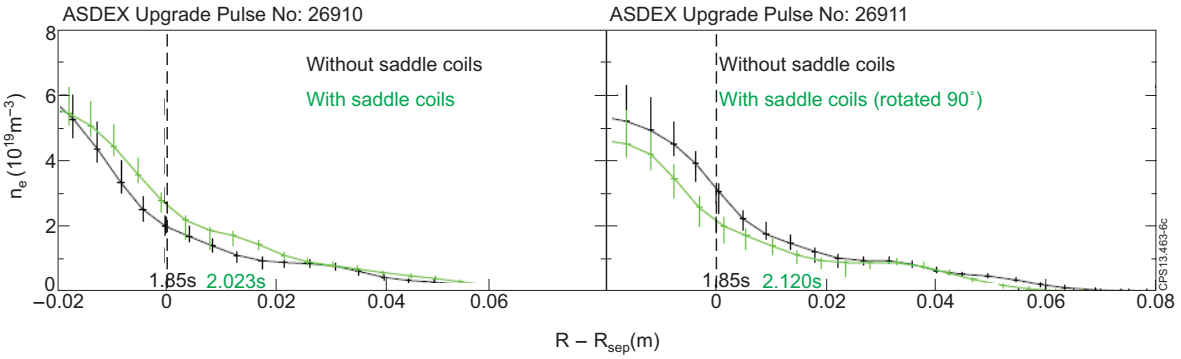

Figure 6. ASDEX Upgrade Density profiles from the lithium beam as a function of the distance to the unperturbed separatrix at the height of the beam at time points between ELMs shortly before (black) and after (green) switching on the saddle coils. The two pictures show shots with the magnetic perturbation rotated by 90°.

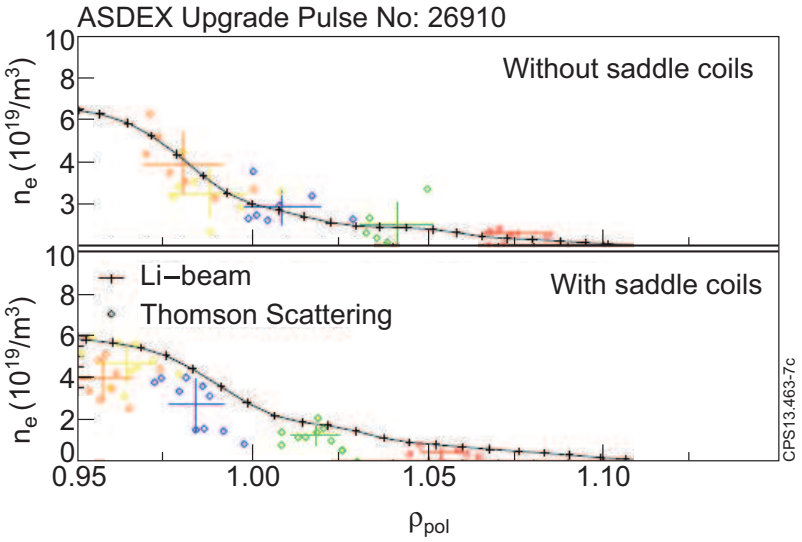

Figure 7. ASDEX Upgrade Mapping of the density measurements from Li-Beam (black) and Thomson-Scattering (coloured, each colour denotes one channel) on the normalised poloidal flux radius. Thomson Scattering measurements are averaged over 100ms, using only time points between ELMs.

Figure 7 shows edge density profiles from the Li-beam and Thomson scattering diagnostics mapped onto the poloidal flux radius ρ_{pol}. Whereas the mapping is good without RMPs, the profiles from the two diagnostics seem to be shifted apart when the coils are switched on. This is mostly due to the fact that the toroidal positions of the two diagnostics differ by 137° and see a different shift of the perturbed separatrix, in this case outward for the Li-Beam and inward for the Thomson scattering diagnostic. The displacement between these two sectors, which should see the maximum displacement for an $n = 2$ field, is only ±3mm, which is equivalent to 0.6% of the minor radius [24], significantly less than in DIII-D, JET and MAST.

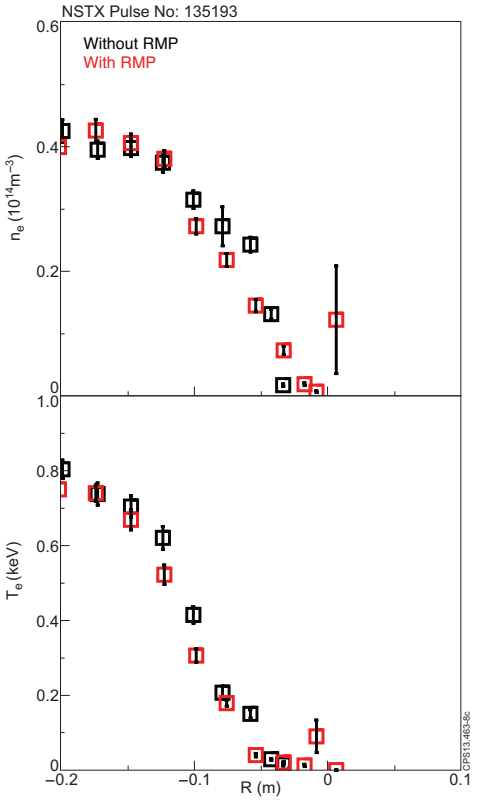

Figure 8. NSTX Thomson scattering measurements of the electron density and temperature profiles in NSTX with and without an $n = 3$ applied RMP, showing negligible displacement caused by the RMP.

A similarly negligible displacement is observed in NSTX when an $n = 3$ RMP is applied from the ex-vessel coils [35], as seen in figure 8. Here, the electron density and temperature profiles are shown (averaged for many time slices both with and without RMPs applied) as measured by the Thomson scattering diagnostic. The displacement is well within the error bars of the diagnostic, so the RMPs have no discernible effect on the boundary.

Overall, there is a wide range of displacements observed in different machines: NSTX and ASDEX Upgrade observe sub-cm displacements for all configurations of applied fields. In contrast, MAST, DIII-D and JET can measure significant displacements, up to $\pm 3.5\%$ of the minor radius when the field is resonant. Furthermore, the amplitude, and even the direction of the boundary displacement is sensitively dependent upon the interaction of the plasma response to the applied non-axisymmetric field and the radial position feedback control system.

2.1. Multi-machine Database

In order to compare the measurements of non-axisymmetric displacements made in different machines, a multi-machine database has been established, incorporating data

from 30 discharges from 5 different machines. The database contains information on I_p, B_t, R_0, a, q_{95}, $n_{e,ped}/n_{GW}$, β_N, b^r_{res} and the measured displacement. There is a very weak correlation between the displacement and all other parameters except for the resonant applied field. For this study, a universal definition of the resonant field is used. Here, b^1 represents the normalised component of the perturbed field perpendicular to equilibrium flux surfaces and is given by $b^1 = (B \cdot \nabla\psi^{1/2}_{pol})/(B \cdot \nabla\phi)$ where B is the total field vector and ϕ is the toroidal angle [34]. The effective radial resonant field component of the applied perturbation normalised to the toroidal field (b^r_{res}) is the amplitude of the resonant Fourier component in the spectrum of b^1 divided by the average value of $\nabla\psi^{1/2}_{pol}$ on the magnetic surface, normalised to the major radius (see page 47 of reference [34]):

$$b^r_{res} = 2|b^1_{m,n}|R_0\langle\nabla\psi^{1/2}_{pol}\rangle \quad (1)$$

Figure 9 shows a linear correlation between the measured 3d displacement (here averaged between all toroidal positions with highly spatially resolved data, removing of course the expected null points) and the resonant field as defined in equation 1. This implies that, whilst vacuum modelling cannot give an accurate determination of the amplitude of the 3d displacement, it can provide a qualitative prediction on the variation of the 3d corrugation with respect to the plasma parameters or the configuration of the applied non-axisymmetric fields. Finally, it is worth noting that there is a very weak correlation between the measured displacements and the normalised pressure in this database. Although this suggests that plasma response is not a leading order parameter in determining the displacements across this multi-machine database, it should be noted that a more appropriate parameter would be $\beta_N/\beta_N^{no-wall}$, since this might be expected to determine the expected plasma response more than the absolute pressure.

At the resonant field expected in ITER, this linear fit would give an empirical scaling for the displacement in ITER of $\pm 2.25\%$ of the minor radius, equating to 9cm peak-to-peak. This means that if the plasma control system were to exacerbate the displacement and apply an $n = 0$ correction to the $n = 3$ or $n = 4$ corrugation, the displacement of the boundary would exceed the limits expected for reliable RF heating coupling and even for heat loads on the plasma facing components. This is far from a robust prediction, but nonetheless, exemplifies why this could be a concern for ITER operation.

3. Modelling of displacements due to RMPs in present machines

The displacements observed in present-day machines presented in section 2 have been modelled using a range of numerical modelling tools – (1) vacuum field line tracing codes giving the change in the position of the magnetic boundary, which is represented by the difference in position of the stable and unstable manifolds when RMPs are applied; (2) ideal three dimensional equilibrium codes, which do not solve the Grad-Shafranov equation, but instead perform an energy-minimisation procedure to find an

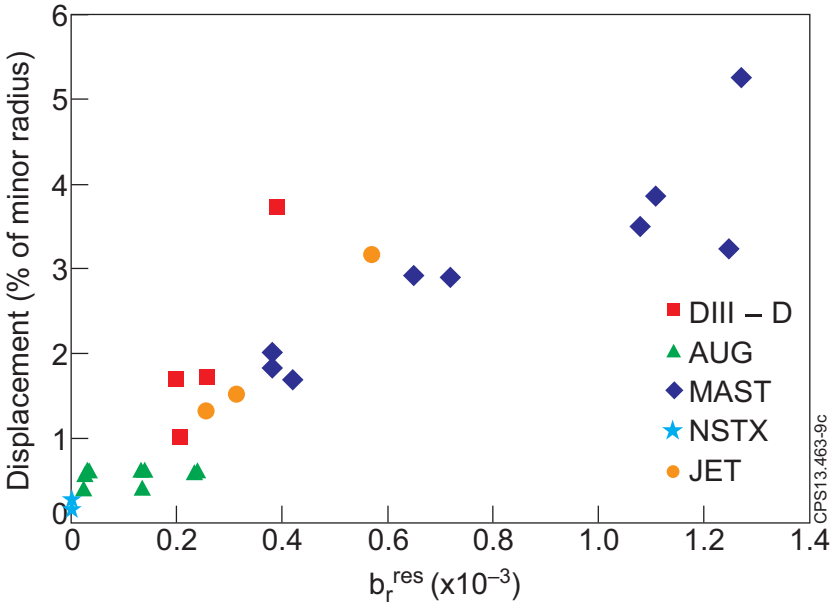

Figure 9. The RMP-induced displacement as a fraction of the minor radius as a function of the resonant applied field at the last rational surface as defined in equation 1 for a multi-machine database covering a wide range of q_{95}, RMP toroidal mode number and spectrum, and β_N

equilibrium state, though the codes used in this study assume ideal, nested flux surfaces; (3) nonlinear MHD codes, which can capture the screening of the applied field, the response of the plasma, the effects of plasma rotation and an X-point geometry. All these models, with very different approaches and different approximations, have been compared to machine data in different parameter space with varying levels of success, illustrating that extrapolation of the 3d corrugation likely in ITER when RMPs are applied is a complex problem.

3.1. Vacuum field line tracing

The simplest prediction for a boundary corrugation comes from vacuum field line tracing, ignoring the plasma response and the shielding of the applied field, which have been shown to be important for understanding ELM behaviour in the presence of RMPs. At the same time, vacuum modelling has also given a reliable prediction for strike-point splitting on the divertor plates, indicating that it can be reliable in the scrape-off layer and right at the plasma edge at least. To some extent, the applicability of vacuum modelling is also confirmed by figure 9 which shows a strong correlation between the resonant field given by vacuum modelling and the measured corrugation of the plasma boundary across 5 different machines. Figure 10 shows a laminar plot illustrating the connection length of field lines from a vacuum field line tracing calculation with an $n = 2$ RMP applied in ASDEX Upgrade [24]. The dashed black line is an effective plasma boundary, marking the envelope of the stable and unstable manifolds, which can be

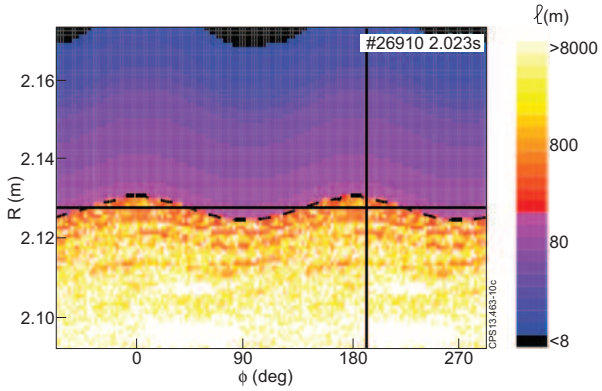

Figure 10. ASDEX Upgrade The plasma boundary predicted by the a field line tracing calculation as a function of toroidal angle for ASDEX Upgrade shot 26910 with an $n = 2$ RMP applied, showing the perturbed boundary compared to the position of the separatrix before RMPs are applied (solid black line). Connection length to the low field side target for field lines starting at a horizontal plane at $z = 0.326$m (height of the lithium beam) around the torus. Marked are the position of the lithium beam at 193° and the unperturbed separatrix at R=2.125m. The dotted line marks the position of the 'perturbed separatrix'.

compared to the solid black line marking the position of the axisymmetric separatrix. There is a toroidal corrugation, though it is only ±3mm, which agrees well with the sub-cm boundary displacement observed experimentally, as seen in figure 6.

In order to confirm this prediction, another independent vacuum field line calculation for ASDEX Upgrade has been performed with the ERGOS code [34]. Figure 11 shows the plasma boundary prediction in a laminar plot produced by ERGOS when either even parity of odd parity $n = 2$ RMPs are applied. For this equilibrium, the even parity case is well aligned with the equilibrium q-profile, as evidence by the larger corrugation amplitude, though in both cases the displacements are predicted to be sub-cm, in line with figures 10 and 6.

However, there are examples where vacuum modelling somewhat under predicts the displacements seen experimentally. For instance, the displacements seen when rotating $n = 2$ RMPs are applied in DIII-D are compared to predictions from the TRIP3D-MAFOT vacuum magnetic field model in figure 12 [28]. The vacuum modelling predicts only ±2.5mm displacement whereas the BES measurements give $\pm 0.8 - 1.2$cm, representing a factor of 4-5 times larger than the vacuum prediction. Whilst the vacuum prediction does not include any screening effects, it also neglects the amplification from the plasma response, which seems to be important in this case. It is shown later that these DIII-D measured displacements are replicated by a nonlinear MHD model which incorporates such plasma amplification effects [39].

A similar under prediction of the boundary corrugation is given by vacuum modelling of MAST discharges with an $n = 3$ RMP applied. Figure 13 shows a laminar plot from ERGOS vacuum modelling from which the vacuum prediction of

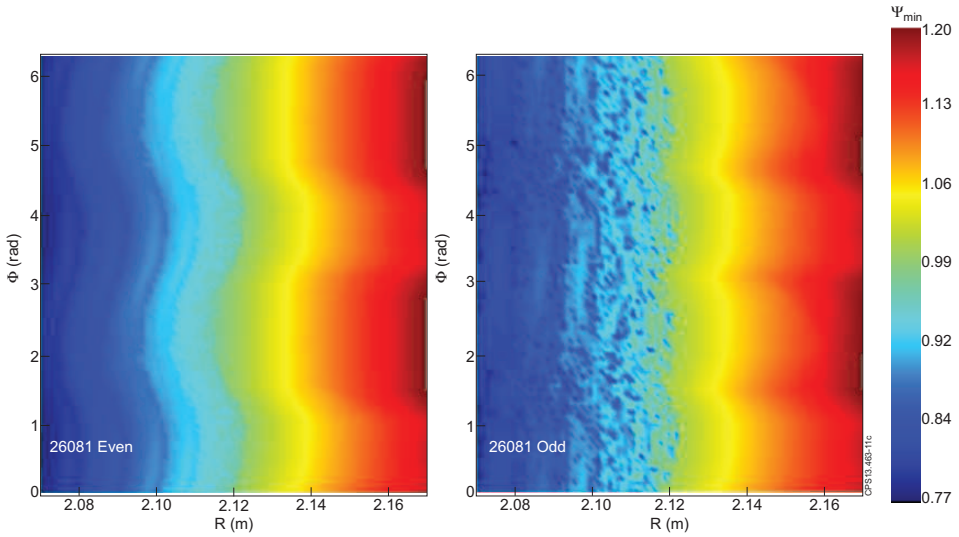

Figure 11. ASDEX Upgrade The plasma boundary predicted by the ERGOS code as a function of toroidal angle for ASDEX Upgrade shot 26081 when either (left) even parity or (right) odd parity $n = 2$ non-axisymmetric fields are applied

the displacement can be inferred. The experimental measurements show a boundary shift of ± 2.5cm [26], which is a factor of four larger than the vacuum prediction of $\pm 5 - 6$mm shown in figure 13.

Whilst vacuum modelling predicts the edge displacement in ASDEX Upgrade accurately, it cannot explain the larger displacements observed in MAST or DIII-D. In order to compare these cases directly, the resonant field in MAST and ASDEX Upgrade is compared using the same vacuum field line tracing code, ERGOS, as shown in figure 14. It is evident that the application of $n = 6$ RMPs in MAST leads to a factor of five larger local resonant field than the $n = 2$ field applied in ASDEX Upgrade. This larger resonant field partially explains why the MAST plasmas experience larger edge corrugations, though the underprediction afforded by vacuum modelling in figure 13 suggests that there is a plasma amplification of the applied field as well.

3.2. Ideal three dimensional equilibrium reconstruction

The next level of complexity in modelling 3d displacements is ideal 3d equilibrium reconstruction. Displacements of the plasma boundary equating to less than 1% of the minor radius observed experimentally are also replicated using such 3d equilibrium modelling in both ASDEX Upgrade and in NSTX. Figure 15 shows the toroidal dependence of the position of the plasma boundary predicted by the VMEC 3d equilibrium code when an $n = 3$ RMP is applied in NSTX [35]. It is evident that the boundary is expected to be perturbed by only ± 1mm, in good agreement with the measured invariance of the pedestal foot position seen in figure 8.

However, in contrast to vacuum modelling, three dimensional ideal equilibrium

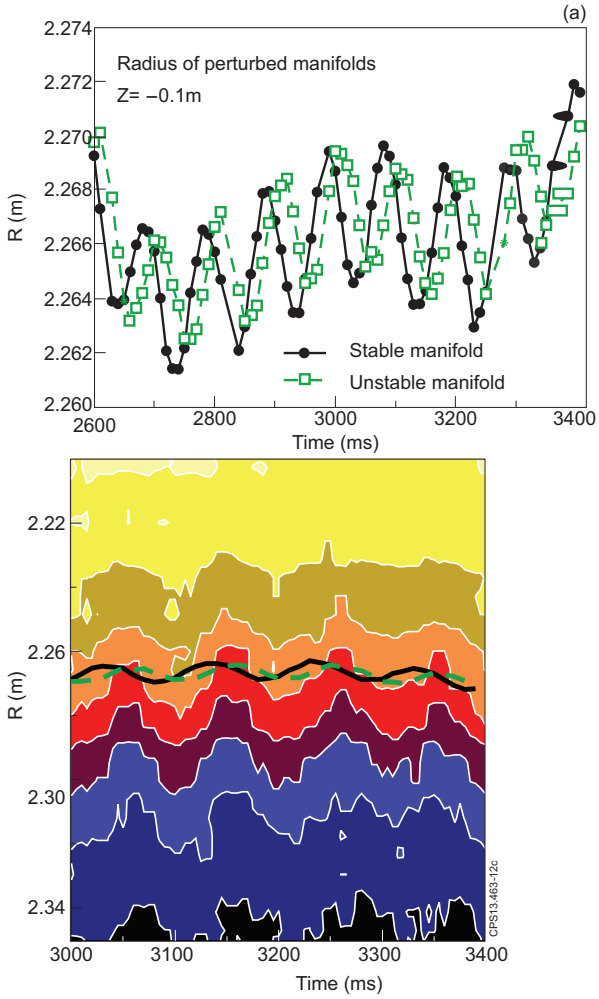

Figure 12. DIII-D (a) Temporal evolution of the major radius R of the (filled black circles and solid black line) stable and (open green squares and green dashed line) unstable manifolds at an elevation of $z = -0.1$m on the LFS midplane computed by the TRIP3D-MAFOT vacuum magnetic field model (no plasma response). Each manifold is displaced by 4-5mm over a cycle of the $n = 2$ RMP rotation. (b) Colour contour plot of the beam emission intensity at an elevation $z = -0.1$m versus R and time in the LFS boundary, showing the displacement in the beam emission profile. The measured BES displacement is compared with the major radius R of the (black solid line) stable and (green dashed line) unstable manifolds at an elevation of z = -0.1m that result from the splitting of the divertor separatrix due to the non-resonant interaction with the $n = 2$ magnetic perturbation. The BES displacement of 1.8-2.4 cm over 18 cycles of the $n = 2$ rotation is $4 - 5$ times the predicted vacuum magnetic field model displacement.

calculations also give good agreement with experimental cases where larger boundary perturbations are observed. Figure 16 shows STELLOPT predictions for the plasma boundary displacement as a function of toroidal and poloidal angles in a DIII-D plasma when an $n = 3$ RMP is applied. The STELLOPT code [40] is designed to optimise the VMEC 3D MHD equilibrium to a set of target physics parameters derived from

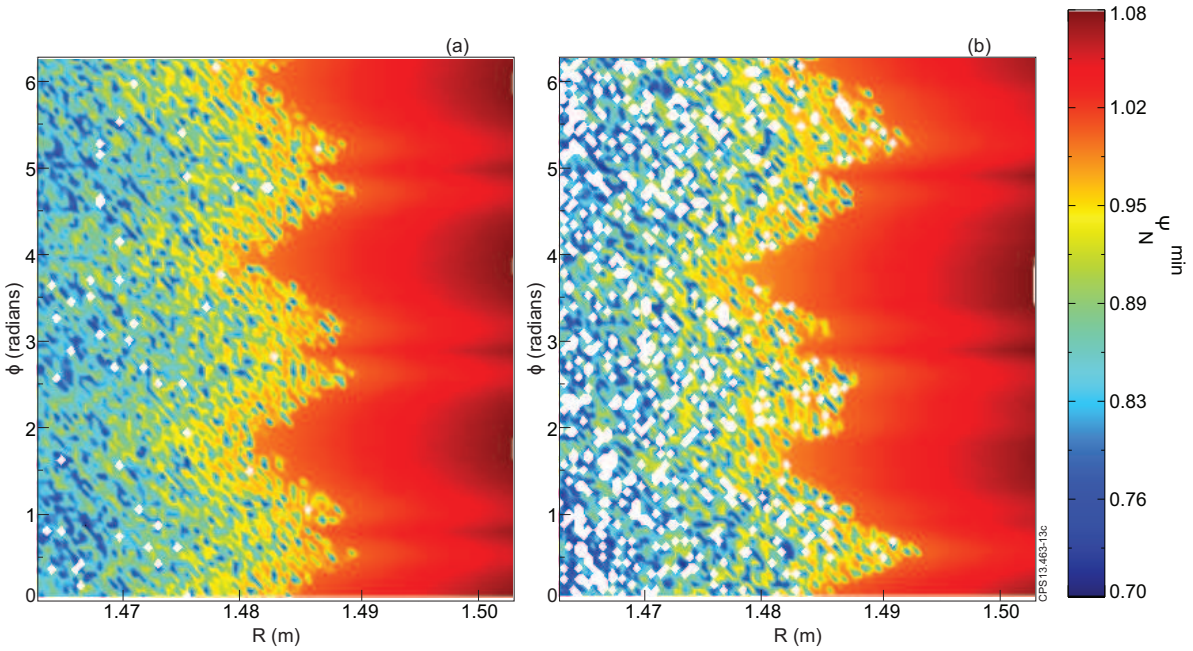

Figure 13. MAST A laminar plot showing the deformation of the 'boundary' in MAST when an $n = 3$ (a) even parity and (b) odd parity RMP is applied as predicted by ERGOS is $\pm 5 - 6$mm, which is significantly less than the displacement measured experimentally [26], where a displacement of ± 2.5cm is observed when the RMPs are switched on.

Figure 14. ASDEX Upgrade and MAST The resonant component of the applied magnetic field as a function of the minor radius as predicted by the ERGOS vacuum field line following code for a MAST connected double null plasma with an $n = 3$ RMP applied and a MAST singlt null plamsa with an $n = 6$ RMP applied compared to ASDEX Upgrade plasma with $n = 2$ field applied with either odd or even parity.

different plasma diagnostics. The reconstruction predicts a boundary corrugation of $\pm$6mm, maximised on the low-field side midplane, in good agreement with measured displacements [41].

Ideal 3d equilibrium reconstruction has also been applied for MAST plasmas when RMPs are applied. Figure 17 shows the radial position of the last closed flux surface at the outboard midplane as predicted by VMEC when an $n = 3$ RMP is applied to a connected double-null MAST plasma where ELM mitigation is observed [12]. Without an applied $n = 3$ field, there is a natural $n = 12$ boundary corrugation associated with the toroidal field ripple, though this is only $\pm$2mm, well below the resolution of any diagnostic. However, when an $n = 3$ field is applied, there is a clear edge corrugation of $\pm$7mm, which is maximised at the midplane.

This can be compared to the edge corrugation predicted by VMEC when an $n = 6$

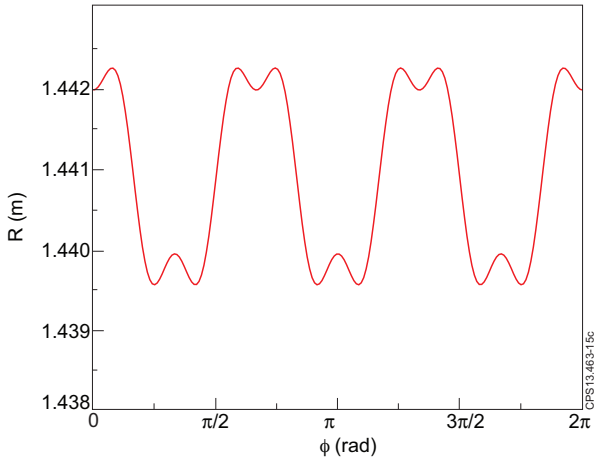

Figure 15. NSTX The toroidal dependence of the radial position of the plasma boundary as predicted by VMEC when an $n = 3$ RMP is applied in NSTX. There is an $n = 12$ toroidal field ripple in addition to the non-axisymmetric $n = 3$ structure.

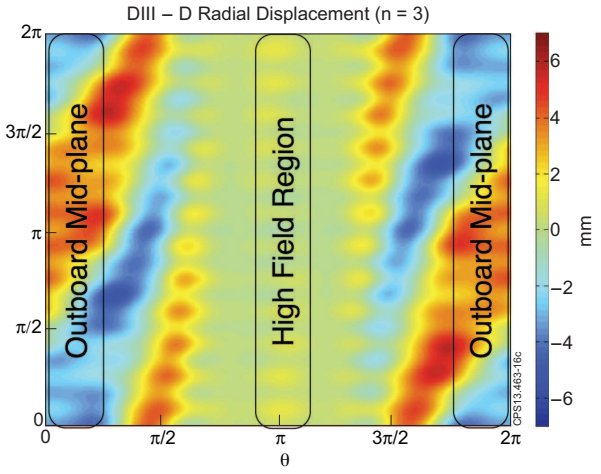

Figure 16. DIII-D The plasma boundary displacement as a function of toroidal and poloidal angles as predicted by the STELLOPT code for a DIII-D plasma with an $n = 3$ RMP applied.

RMP is applied to a connected double null MAST plasma, as shown in figure 18. It is evident that the boundary corrugation resultant from the $n = 6$ RMPs is strongly dependent on the alignment of the applied field with the equilibrium field. In the case of the even parity field, there is negligible distortion, whereas the odd parity $n = 6$ RMP gives rise to a ±1cm corrugation.

When the applied field is optimally aligned with the plasma field– at which point the ELM mitigation is maximised [12] – the corrugation is even larger. Figure 19 shows ANIMEC modelling of a MAST connected double null plasma when an $n = 3$ field is applied with a pitch angle to align the field with the q-profile. In this case the edge corrugation is ±2.5cm, equating to ±4.5% of the minor radius. Also shown in figure 19

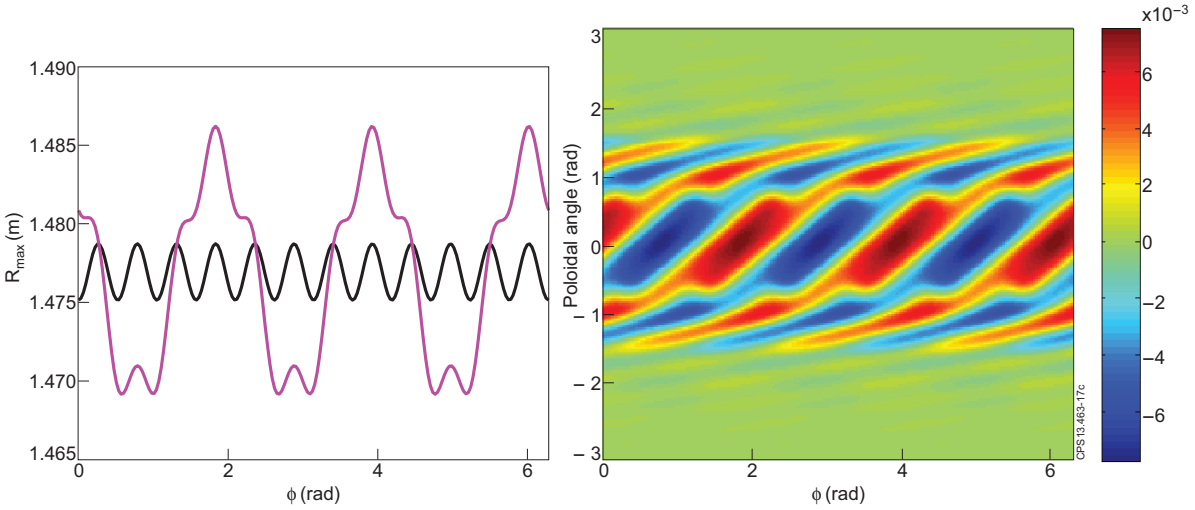

Figure 17. MAST (left) The plasma boundary predicted by VMEC for a MAST connected double null plasma when an n=3 RMP is applied (pink) compared to the case with no RMP but with toroidal field ripple (black). (right) The boundary displacement predicted by VMEC as a function of toroidal and poloidal angle, showing maximum displacement on the midplane for this double-null plasma.

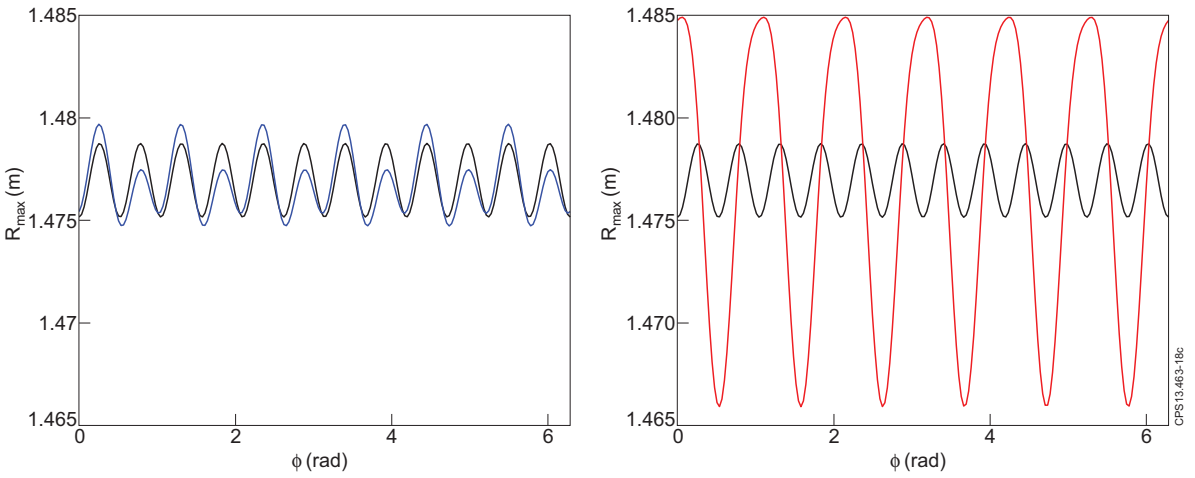

Figure 18. MAST The plasma boundary predicted by VMEC for a MAST connected double null plasma when an n=6 RMP is applied compared to the case with no RMP but with toroidal field ripple when the RMP has (left) even parity configuration and (right) an odd parity configuration.

are data from different diagnostics in MAST when this phase of $n = 3$ RMP is applied, showing excellent agreement between the measured position of the plasma boundary and the predicted edge position from ANIMEC, suggesting that ideal 3d MHD equilibrium reconstruction is able to replicate the experimental shifts observed in MAST accurately.

However, there are examples where ideal 3d equilibrium reconstruction does not replicate the large boundary corrugations observed in some experiments. For instance,

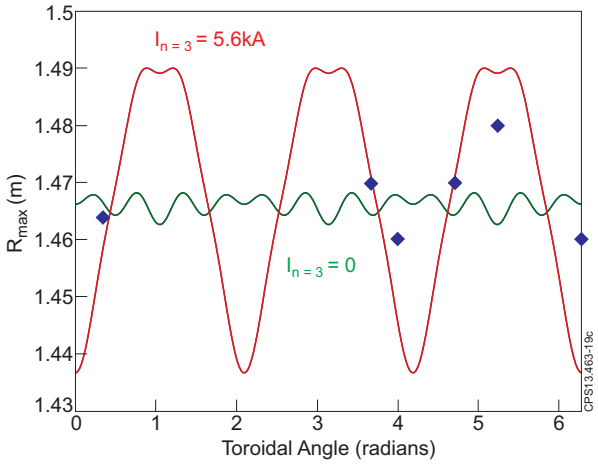

Figure 19. MAST The plasma boundary displacement as a function of toroidal angle as predicted by the ANIMEC code compared to measurements of the midplane displacement in MAST when an $n = 3$ RMP is applied.

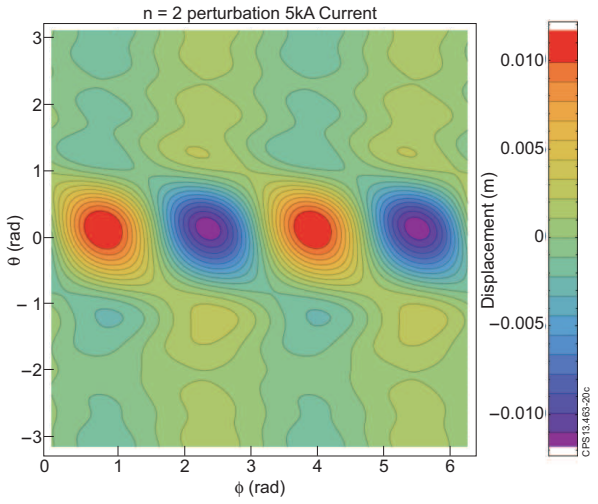

Figure 20. JET The plasma boundary displacement as a function of toroidal and poloidal angles as predicted by the VMEC code when an $n = 2$ RMP is applied in JET.

figure 20 shows a VMEC 3d equilibrium for a JET plasma with 80kAt in the external coils producing an $n = 2$ field. This $n = 2$ RMP is observed to produce a boundary displacement of ±3cm [32], whereas VMEC predicts only a ±1cm boundary corrugation for this plasma equilibrium.

Similarly, it can be seen by comparing figure 16 with figure 5 that the STELLOPT 3d equilibrium reconstruction produces slightly smaller displacements at the boundary than those which are measured experimentally in DIII-D (though it is worth noting that it produces a much better agreement than the factor of four discrepancy with vacuum modelling seen in figure 12).

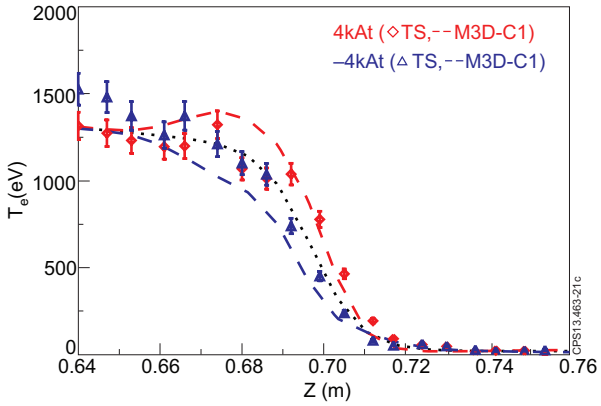

Figure 21. DIII-D The electron temperature profile as a function of Z as measured by the Thomson scattering diagnostic in DIII-D (symbols) compared to the prediction from the M3D-C^1 linear MHD code for two phases of an applied $n = 3$ RMP, showing good agreement and a clear edge displacement.

3.3. Resistive MHD modelling

The next level of complexity is to use a resistive MHD model which includes the plasma response to the applied field, allowing amplification by marginally stable MHD modes as well as screening of the field. Figure 21 shows such a comparison between the electron temperature pedestal measured by the Thomson scattering diagnostic in DIII-D and that predicted by the M3D-C^1 MHD code. In this case, the displacements observed experimentally are accurately modelled by linear resistive MHD.

Furthermore, M3D-C^1 is also able to replicate the dependence of the corrugation amplitude on plasma parameters. In DIII-D, larger displacements are observed at larger q_{95}: plasmas with $q_{95} = 3.1$ have $\xi_a \approx 4$mm whereas plasmas at $q_{95} = 3.8$ have $\xi_a \approx 8$mm. Such a dependence on plasma current is replicated by M3D-C^1 as shown in figure 22. This trend follows the vacuum field intuition, since $\delta B/B$ (via I_{RMP}/I_P) increases with q_{95}, here changed by scaling the current. Indeed, vacuum modelling based on these shots recovers this trend [42]. It is contrary, however, to the intuition one might apply if plasma amplification plays a key role in determining the edge displacement. One might assume that higher current sustains higher pressure gradient, making edge modes more unstable, hence amplifying the applied field and leading to *larger* displacements, rather than the smaller edge corrugation observed. However, resistive MHD including rotation is able to capture both amplification and screening and as such includes the pertinent physics to allow good agreement across a wide range of plasma conditions.

The simulations in figures 21 and 22 use a linear MHD approximation. Here we consider linear modelling as appropriate provided $|\mathrm{d}\xi_r/\mathrm{d}r| < 1$. If this condition is not met, then the flux surface displacements overlap, implying a breakdown of the condition $B \cdot \nabla T_e = 0$. In order to verify the applicability of the linear model in these conditions, the displacements predicted using linear MHD have been compared to non-linear simulations, as shown in figure 23. The overlap criterion that $|\mathrm{d}\xi_r/\mathrm{d}r| < 1$

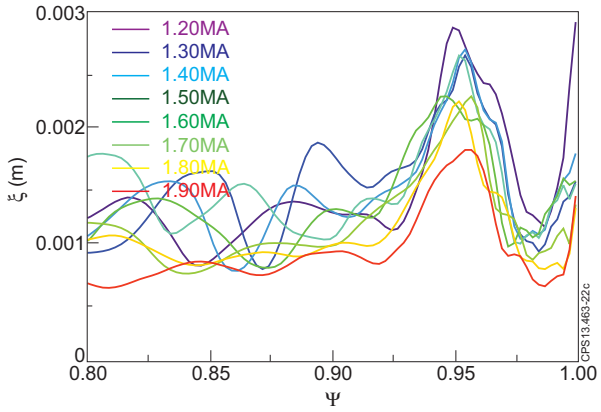

Figure 22. DIII-D The flux surface perturbation as a function of radius for different values of plasma current with an applied $n = 3$ RMP, as modelled by linear M3D-C^1 runs. It is clear that the edge displacement increases for lower I_p, that is to say for higher q_{95} in this case.

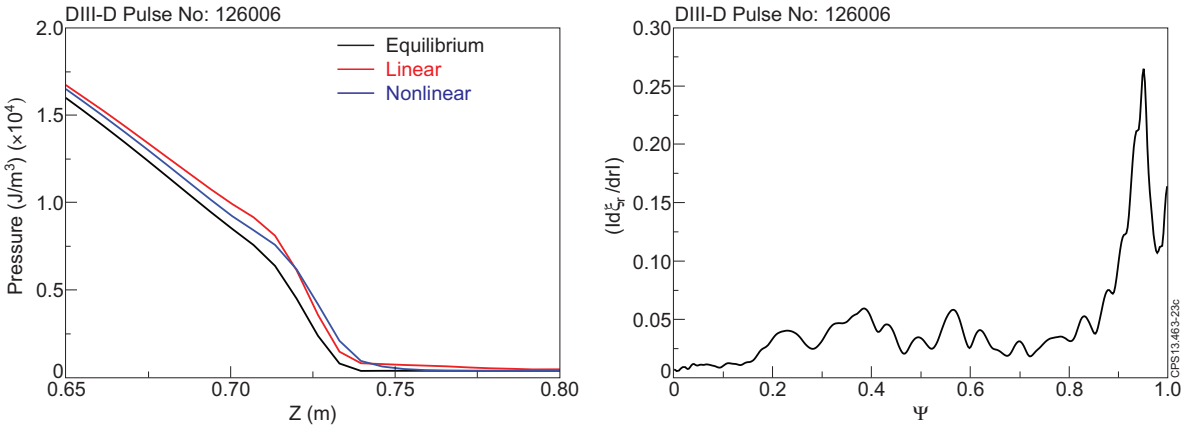

Figure 23. DIII-D The plasma electron pressure as a function of vertical position (along the line of sight of the Thomson scattering) in DIII-D as predicted by the M3D-C^1 code, comparing the results of linear and non-linear simulation when an $n = 3$ RMP is applied.

is clearly met across the whole minor radius, and commensurately, the boundary displacements, and indeed the whole pedestal electron temperature profile, is in good agreement in the linear and nonlinear simulations.

Another nonlinear resistive MHD code, JOREK [43], has been used to simulate MAST [54] and JET plasmas [38] when RMPs are applied. JOREK simulations with realistic resistivity and flows have been performed for JET discharges with an $n = 2$ RMP applied. For discharge 77329, the measured displacement resulting from the application of the $n = 2$ RMP is ±1cm. Figure 24 shows the predicted displacements at the plasma top, X-point and midplane respectively when JOREK is run without realistic diamagnetic and toroidal flows included. In this case the boundary displacement is ±1.2cm. When realistic flows are included in the simulation, the boundary displacement

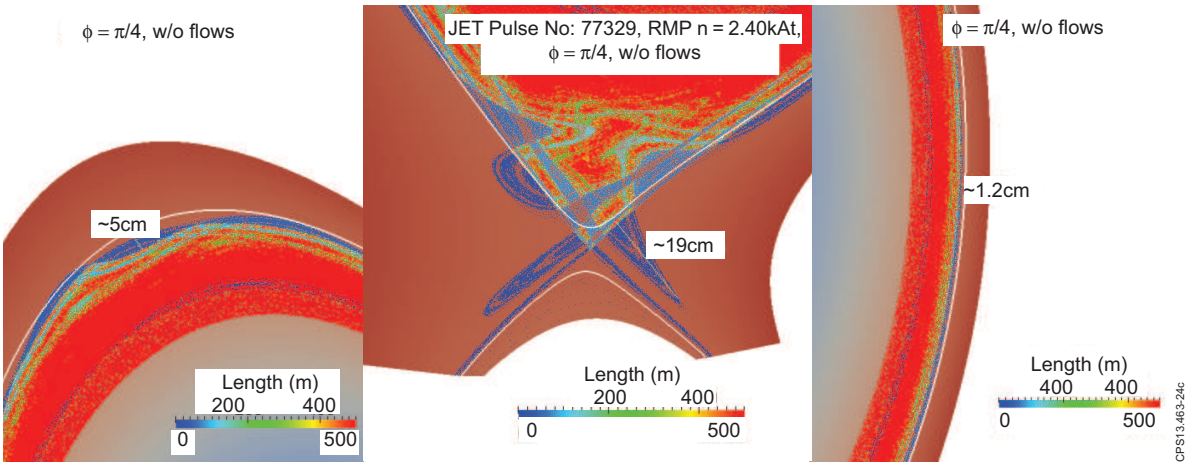

Figure 24. JET Poincare plots showing the (left) top, (middle) lower X-point region and (right) midplane of JET discharge 77329 modelled using JOREK without realistic diamagnetic and toroidal flows included.

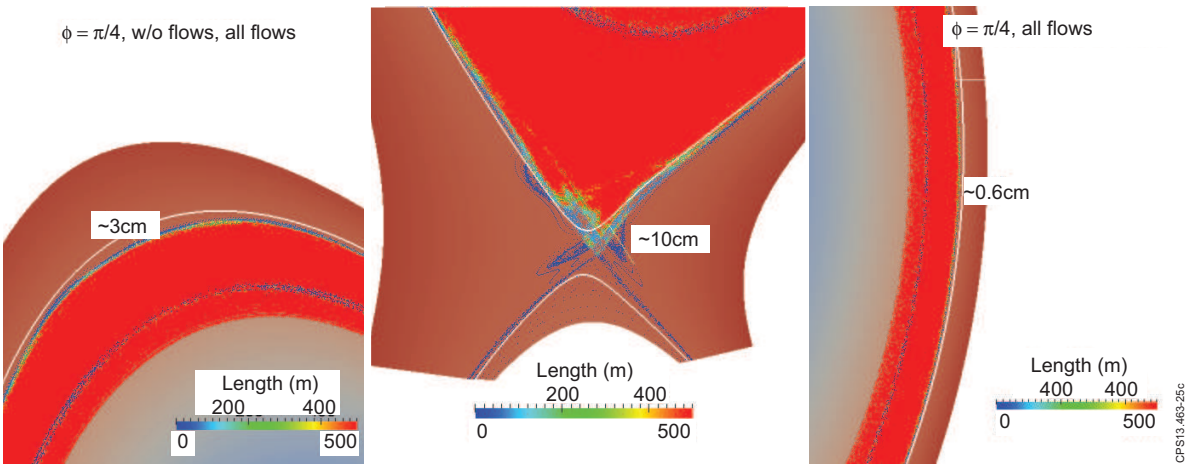

Figure 25. JET Poincare plots showing the (left) top, (middle) lower X-point region and (right) midplane of JET discharge 77329 modelled using JOREK when realistic diamagnetic and toroidal flows are included.

is halved, to ±6mm, as shown in figure 25.

3.4. Comparison of different numerical models

In section 2 the range of measured displacements in present day machines was detailed, ranging from ±3.5% of the minor radius to negligible edge corrugation. In a similar vein, the models needed to replicate the experimental observations range from simple vacuum field line tracing, to ideal 3d equilibria and nonlinear resistive MHD simulations. Whilst there is a strong correlation between the resonant field predicted by vacuum models and the measured displacement, seen in figure 9, vacuum modelling does not

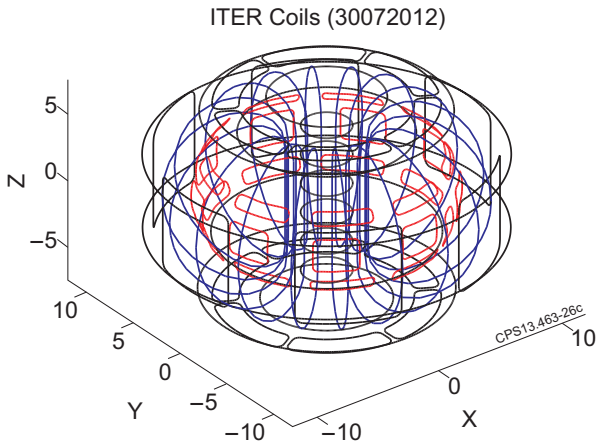

Figure 26. The coil set used in ITER simulations.

always accurately replicate the absolute magnitude of the empirical observations, even if it does provide qualitative trends with respect to the plasma parameters. Indeed, in all cases where large displacements are observed, either ideal 3d equilibrium reconstruction (in MAST) or resistive MHD including plasma amplification effects (in DIII-D and JET) are required to replicate the observations. However, there remains uncertainty in all of these models, in the level of plasma and rotation screening of the applied fields, in the damping caused by the applied field and in the nonlinear interaction of 3d fields, marginally stable modes and rotation. Therefore it is prudent to use all models available and take the worst case scenario when making predictions for ITER, as follows in section 4.

4. Modelling of displacements due to RMPs in ITER

As in section 3, the displacements expected in ITER are modelled using vacuum field line tracing, ideal 3d equilibrium reconstruction and nonlinear resistive MHD codes. The coil set used in these simulations is shown in figure 26, including the latest design for the in-vessel control coils (IVCCs) planned for ITER.

4.1. Vacuum field line tracing

The TRIP3D vacuum field line tracing code has been used to predict the boundary displacement expected in a 15MA baseline scenario when full current is applied in the IVCCs in an $n = 3$ configuration. Figure 27 shows the radial position of the axisymmetric plasma boundary in the absence of RMPs compared to the position of the unstable and stable manifolds resultant under the application of a non-axisymmetric field perturbation. In plasma simulations one can take an isotherm or isobar as a proxy for the boundary position. The boundary location is somewhat harder to define in vacuum modelling. Non-axisymmetric magnetic perturbations split the separatrix into

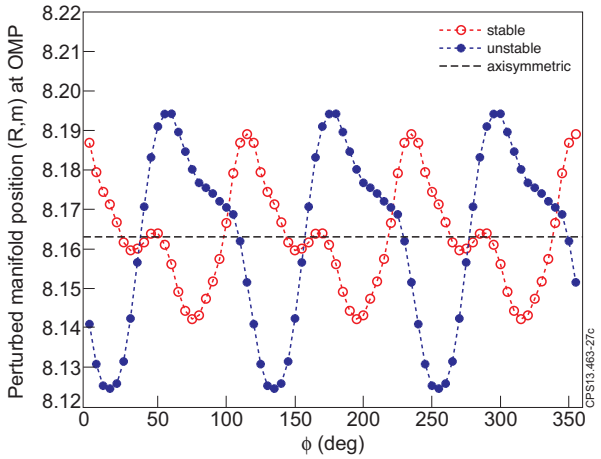

Figure 27. ITER The radial position of the axisymmetric plasma boundary in ITER 15MA baseline scenario predicted by TRIP3D vacuum field line tracing code, compared to the unstable and stable manifold positions when a full-field $n = 3$ RMP is applied.

stable and unstable manifolds [44, 45], with corrugated structures forming where these manifolds intersect. These homoclinic tangles are computed to be particularly complex and extended near the X-point. This concept of lobe structures formed by the invariant manifolds of the perturbed field has been used to explain the splitting of the divertor leg footprints observed on strike-point targets during RMP experiments [46, 47, 48, 44, 49], suggesting that at least for the boundary and scrape-off layer, vacuum modelling gives a good description of the effect of the applied fields. Furthermore, vacuum modelling with an appropriate screening model has been used to get a good correspondence between the X-point lobe strcutures measured in MAST [11, 55]. Using the difference between the stable and unstable manifolds as a proxy for the boundary position, it is evident from figure 27 that simple vacuum modelling suggests a corrugation of ±3cm, representing ±1.5% of the minor radius in ITER 15MA baseline plasmas, though it should be noted that this does not include any plasma screening of the applied field.

It is possible to use a simple analytic model to find the dependence of the boundary displacement on the equilibrium q-profile, and thus on the resonance of the applied field. We start by taking the 3D magnetic perturbation spectrum from an M3D-C^1 response calculation for the baseline ITER scenario with a 3.8keV pedestal temperature and 22.5kAt in the midplane-IVCCs. The outermost radial point in the domain is chosen, at $\psi_N = 0.9988$ and $q = 4.262$. Three dimensional local equilibrium theory is used to study the sensitivity of the 3D deformation size at this surface to the local value of the safety factor. Starting with the axisymmetric flux surface shape (taken from the initial 2D equilibrium used in the M3D-C^1 response calculation), we add a spectrum of 3D flux surface deformations which match the 3D radial magnetic perturbation spectrum from M3D-C^1. This approach follows the procedure described in reference [36]. In the high aspect ratio, circular cross section limit the relationship between a deformation of a given helicity (γ) and the radial magnetic perturbation with which it is associated is

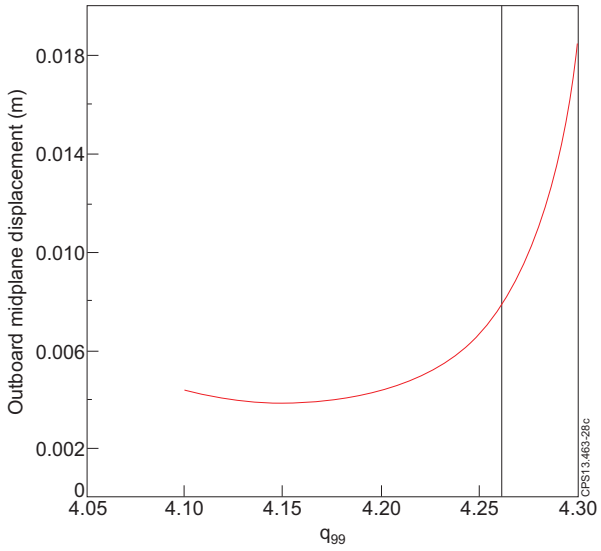

Figure 28. ITER The edge displacement as a function of the edge safety factor found from simple 3d local equilibrium theory.

given by $B_r/B_0(m,n) = (\gamma/R_0)(nq-(m-1))$, where an $m = 4$ deformation is associated with an $m = 3$ radial magnetic perturbation. With the q value taken from the response calculation we find a 3D flux surface displacement at the outboard midplane of $\pm$7mm. We then repeat the calculation of the flux surface displacement with varying safety factor, but holding the 3D perturbation spectrum fixed. The energy needed to bend equilibrium magnetic field lines decreases as low order rational surfaces are approached, and consequently the displacement size has a $1/x$-type sensitivity where x is the distance to the nearest low order rational surface. The validity of these calculations comes into question as the rational surface is approached, as the resonant component of the radial magnetic perturbation may be suppressed by flow screening, and in principle new radial perturbation spectra should be used. Here we limit our calculations to a range of q values where the radial magnetic perturbation spectra used should remain valid. These calculations suggest that the displacement of the last closed flux surface will have some sensitivity to the q value, as seen clearly in figure 28. Small changes in the edge q value may be able to significantly modify the displacement of the last closed flux surface.

4.2. Ideal three dimensional equilibrium reconstruction

3d equilibrium reconstruction of the various ITER scenarios with either $n = 3$ or $n = 4$ RMPs applied has been performed using the VMEC code. The profiles for the baseline scenario are taken from the latest transport simulations of ITER 15MA plasmas using the CORSICA code [50].

The NEMEC code (a free boundary version of VMEC, which for the purposes of this study is ostensibly identical and checked against VMEC [53]) has been used to assess the boundary displacements in various ITER scenarios with both $n = 3$ and $n = 4$

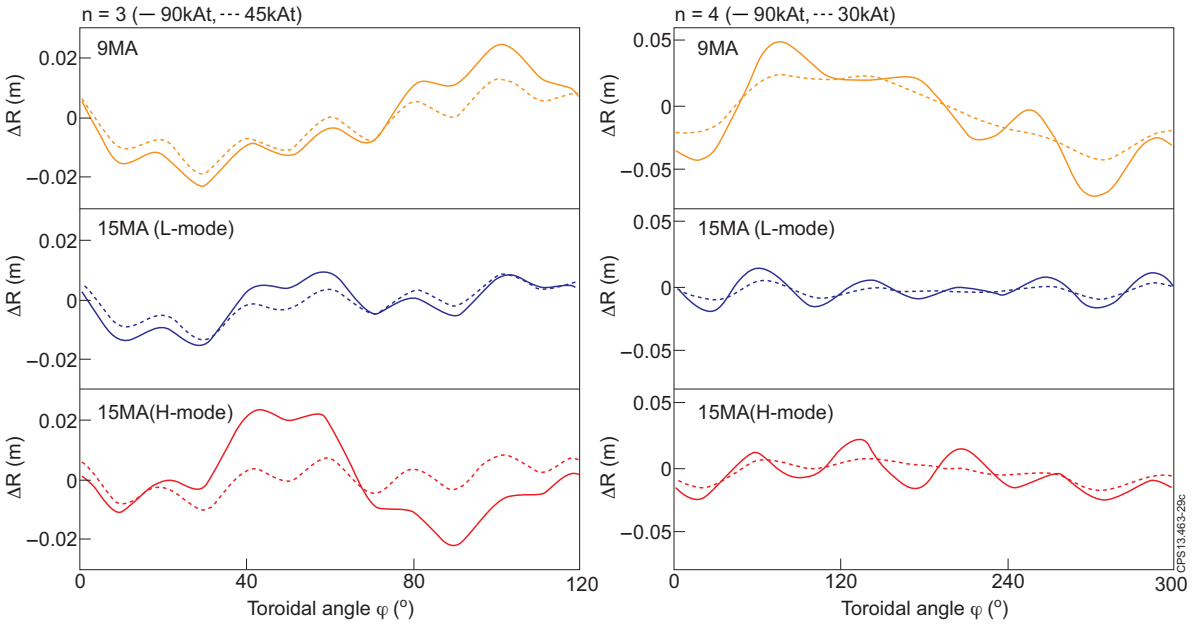

Figure 29. ITER The midplane plasma boundary displacement as predicted by NEMEC for the (top pane) ITER 9MA scenario, (centre pane) 15MA L-mode phase and (bottom pane) 15MA H-mode phase as modelled with CORSICA. All twelve calculations are shown. The 90kAt calculations are indicated by solid lines, the calculations with 45kAt in the n=3 cases (left column) and the results with 30kAt in the n=4 cases (right column) by dashed lines.

applied RMPs at different field strengths. The simulations naturally include TF ripple effects (without ferritic inserts), which alone can induce corrugations of $\pm 7-8$mm. Four current distributions in the IVCCs have been studied, namely an $n = 4$ configuration with $I_{IVCC} = 90$kAt and $I_{IVCC} = 30$ kAt and an $n = 3$ configuration with $I_{IVCC} = 90$ kAt and $I_{IVCC} = 45$ kAt [51]. The $n = 4$ cases show a strong addition of $n = 5$, whilst the $n = 3$ cases have additional $n = 6$ amplitudes. In all twelve NEMEC calculations (two coil configurations $\times$ two RMP amplitudes $\times$ three plasma scenarios – 9MA flat-top, 15MA L-mode and 15MA H-mode flat-top) the outer plasma edge in the $Z = 0$ plane is displaced by several centimetres, shown in figure 29. The toroidal dependence of the displacement is not a pure $n = 3$ or $n = 4$ due to the rather impure spectrum applied from the IVCCs together with the TF ripple. For the $n = 4$ RMPs with $I_{IVCC} = 90$kAt in the 9MA plasma, the plasma edge is displaced by up to ≈ 5cm from its axisymmetric position. The smallest edge displacement is observed in the 15MA L-mode scenario, for both $n = 3$ and $n = 4$ RMPs, where the corrugation is roughly 1cm if $I_{IVCC} = 90$kAt. Pertinently, the 15MA cases with $I_{IVCC} = 90$kAt in $n = 4$ configuration, as envisaged for baseline $Q = 10$ operation, has a midplane displacement of ± 2cm (or $\pm 1\%$ of the minor radius).

4.3. Resistive MHD modelling

Finally, nonlinear resistive MHD simulations have also been performed for the 15MA ITER baseline scenario with two different codes: M3D-C^1 and JOREK. In principle, these models represent the most accurate representation of the empirical situation and should therefore give greatest fidelity to the experiment and have greatest weight in the prediction for ITER, although the uncertainties in various parameters and profiles which influence the results strongly means that the prediction for ITER still comes with significant uncertainty.

Figure 30 shows the radial displacement across the pedestal region when $n = 1, 2, 3, 4$ RMPs are applied with maximum amplitude (ie $I_{IVCC} = 90$kAt) as predicted by linear M3D-C^1 simulations assuming various values for the pedestal-top temperature [37]. In all cases the boundary displacement increases with the pedestal temperature as the applied field is amplified by increasingly unstable low-n peeling modes at the plasma edge. For the $n = 3$ and $n = 4$ configurations (as intended for ELM control) the boundary displacement can exceed 5cm for high pedestal pressures. However, it is important to note that the overlap criterion for the validity of linear simulations, $|\mathrm{d}\xi_r/\mathrm{d}r| < 1$, is violated for $T_{e,ped} = 5.1, 6.0$keV [37]. Nonetheless, even at $T_{e,ped} = 4.4$keV, which is assumed as the operating point for $Q = 10$ baseline scenario [52], both the $n = 3$ and $n = 4$ RMPs lead to a boundary displacement of $\pm\xi_a = 3.5$cm, or $\pm 1.75\%$ of the minor radius.

Figure 31 shows a comparison of the pressure predicted by the linear and nonlinear response calculations with M3D-C^1 at $Z = 0$ at two different toroidal positions in ITER baseline scenario. In this case a 3.8keV pedestal is assumed with an $n = 3$ RMP applied at full coil current. Both calculations used the same transport coefficients and mesh and both are single-fluid. The linear and nonlinear simulations give similar pressure profiles, and importantly both show the same direction of the boundary displacement in each toroidal position, though the amplitude of the displacement varies. The difference seems to be that the nonlinear calculation develops significant $n < 3$ response (the applied field is dominantly $n = 3$ with some $n = 6$ sideband). If the response were purely $n = 3$, one would expect that the boundary displacement should be equal and opposite in the two figures; this is (exactly) true for the linear calculation, but it is clearly not the case for the nonlinear calculation. Nonetheless, this comparison suggests that the linear calculations give a good approximation for the boundary displacement (at least for the 3.8keV pedestal which is well below marginal stability), albeit neglecting small corrections from $n \neq 3$ components. In this case, the boundary displacement at the midplane when an $n = 3$ field is applied is $\pm$2cm, equating to $\pm 1\%$ of the minor radius.

The JOREK non-linear MHD code has also been used to simulate the effects of RMPs in ITER [38]. Figure 32 shows a Poincare plot of the magnetic field lines in ITER baseline scenario when diamagnetic flows and realistic toroidal rotation (left) are not included and (right) are included. The displacements near the X-point are

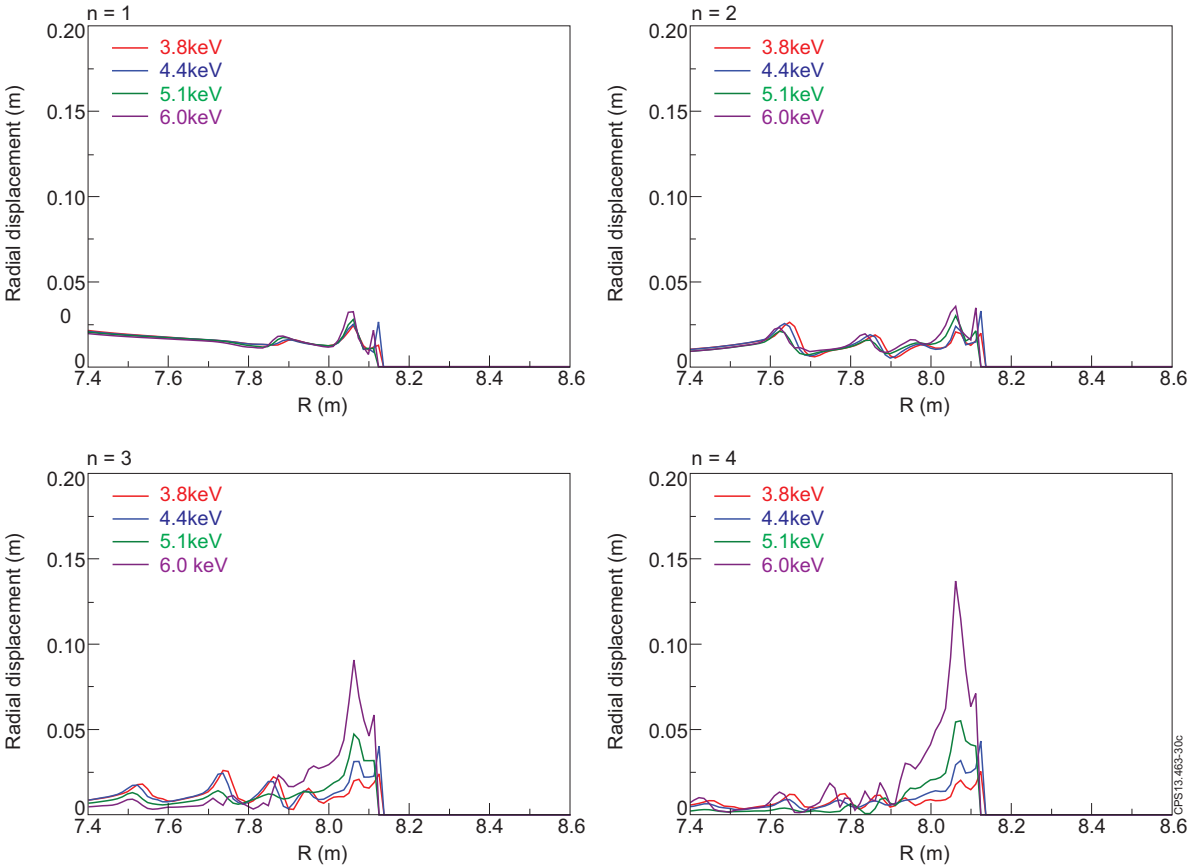

Figure 30. ITER The radial displacement as a function of the major radius in ITER baseline H-mode scenario as predicted by the M3D-C[1] code when 90kAt is applied from the in-vessel coils in $n = 1, 2, 3, 4$ configurations, showing increasing displacement with pedestal temperature.

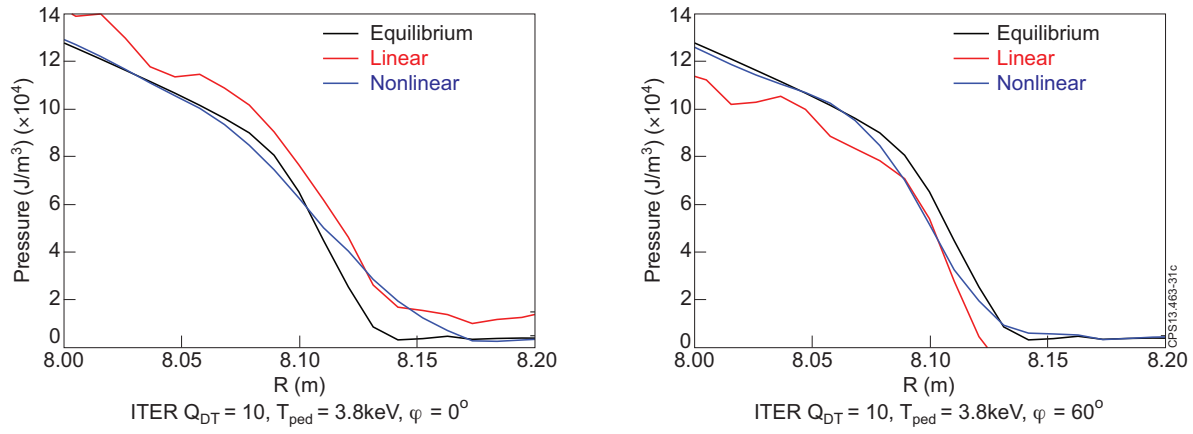

Figure 31. ITER The pressure predicted by the linear and nonlinear response calculations with M3D-C[1] for ITER baseline scenario with a 3.8keV pedestal and an $n = 3$ field applied at full coil current. The two figures show the pressure profile in two toroidal positions 60° apart.

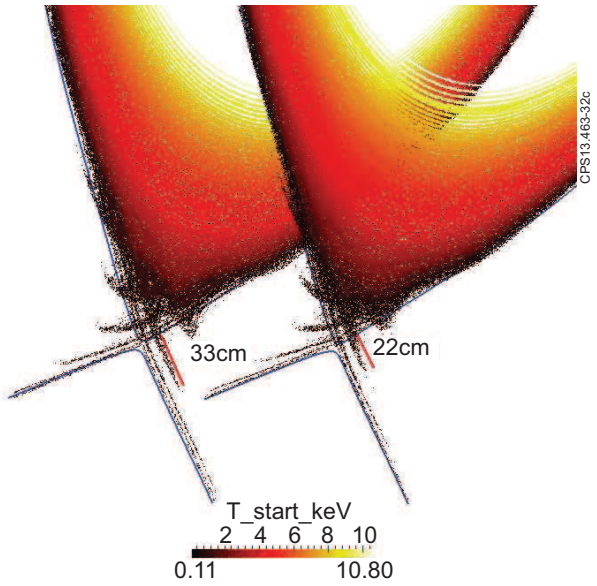

Figure 32. ITER A Poincare plot of the magnetic field lines in ITER baseline scenario when diamagnetic flows and realistic toroidal rotation (left) are not included and (right) are included in JOREK, showing large displacements near the X-points.

significantly radially extended, but the boundary displacements away from the X-point are negligible. Figure 33 shows the electron density and temperature profiles across the pedestal as predicted by JOREK when an $n = 3$ RMP is applied with $I_{IVCC} = 55$kAt, illustrating a boundary corrugation of $\pm$1cm, ie only $\pm$0.5% of the minor radius [38]. Of course this would be expected to approximately double at full applied field, in excellent agreement with the M3D-C^1 results for the same ITER case shown in figure 31, adding credence to this prediction.

4.4. Overview of ITER modelling

A range of numerical models have been used to predict the displacements likely in ITER due to the application of RMPs. Vacuum field line modelling suggests the separatrix deformation will be $\pm$3cm, equating to $\pm$1.5% of the minor radius. Of course, this assumes no plasma screening nor amplification. More sophisticated ideal 3d equilibrium reconstruction predicts that, for the 15MA baseline scenario, both $n = 3$ and $n = 4$ RMPs at full applied field will give rise to $\pm$2cm midplane displacements. This modelling still assumes no screening and does not allow for formation of magnetic islands. Resistive nonlinear MHD modelling using two independent codes, which provide the most complete physical model of the plasma, predicts that for $T_{e,ped} = 3.8$keV, one could expect a midplane boundary displacement of $\pm$2cm. The amplitude of this corrugation increases as the temperature pedestal increases, or as the plasma flows decrease. For

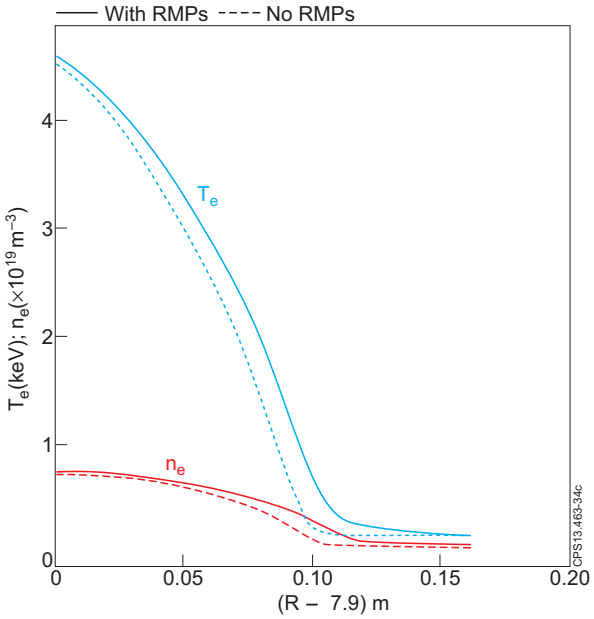

Figure 33. ITER The electron density and temperature as a function of the minor radius as predicted by a non-linear JOREK simulation when 55kAt is applied in $n = 3$ configuration.

$T_{e,ped} = 4.4$keV, as assumed for $Q = 10$ operation [52, 50], the displacement amplitude is ± 3.5cm, comparable to the prediction assuming vacuum field only.

5. Discussion and Conclusions

It is evident that applied non-axisymmetric fields can give rise to significant displacements of the plasma boundary. These displacements have been measured in various tokamaks and successfully compared with numerical simulation. A multi-machine database exhibits a linear correlation between the measured corrugation and the resonant applied field as predicted by vacuum modelling, suggesting that vacuum field line tracing can at least qualitatively replicate the empirical phenomenology. Indeed, in the case of sub-cm displacements in ASDEX Upgrade and NSTX, vacuum models agree quantitatively. However, there are cases in JET, MAST and DIII-D where vacuum modelling significantly under-predicts the corrugation. In these cases, ideal three dimensional equilibrium reconstruction provides greater fidelity with experimental measurements. Even so, there are some empricial measurements at very large displacement – for example the displacements of up to 5cm observed in JET – where only resistive nonlinear MHD models can accurately replicate measurements. Such models including plasma screening, amplification, flows and allowing islands to form are the most representative tools and can reproduce measured corrugations over parameter scans in various machines. The RMP-induced displacements foreseen in ITER are expected to lie within the range of those predicted by the different models, meaning

less than ±1.75% (±3.5cm) of the minor radius in the H-mode baseline and less than ±2.5% (±5cm) in a 9MA plasma.

Such toroidal corrugation of the plasma boundary affects many things, notably the coupling of ICRH, the minimum values of wall gaps assumed for safe operation, the plasma position control, and (de facto) the control of ELMs. Indeed, such a boundary corrugation may be necessary to affect the ELMs [20] and using plasma control feedback to provide an $n > 0$ correction may compromise the efficacy of the RMPs as an ELM control scheme. Whilst a displacement of ±3cm in the baseline scenario is allowable from both a plasma control and heat loading perspective, it is important that ITER adopts a plasma control system which can account for a three dimensional boundary corrugation to avoid an $n = 0$ correction which would otherwise exacerbate the displacement caused by the applied fields.

Acknowledgements

This work was conducted under the auspices of the ITPA MHD Stability Topical Group. This work was part-funded by the RCUK Energy Programme [grant number EP/I501045]; the European Communities under the contract of Association between EURATOM and CCFE, CEA, IPP, CRPP, FZJ and VR; and US Department of Energy under DE-XXXXXXXXX. To obtain further information on the data and models underlying this paper please contact PublicationsManager@ccfe.ac.uk. The views and opinions expressed herein do not necessarily reflect those of the European Commission. This work was carried out within the framework of the European Fusion Development Agreement.

[1] Connor JW, 1998 *Plasma Phys Control Fusion* **40** 531
[2] Snyder PB *et al* 2002 *Phys Plasmas* **9** 2037
[3] Wilson HR *et al* 2006 *Plasma Phys Control Fusion* **48** A71
[4] Suttrop W, 2000 *Plasma Phys Control Fusion* **42** A1
[5] Loarte A *et al* 2003 *Plasma Phys Control Fusion* **45** 1594
[6] Evans T *et al*, 2004 *Phys Rev Lett* **92** 235003
[7] Evans T *et al* 2008 *Nucl Fusion* **48** 024002
[8] Jeon YM *et al* 2011 *Proc. 53rd Annual Meeting of Division of Plasma Physics (AIP)* T04.00005
[9] Suttrop W *et al* 2011 *Phys Rev Lett* **106** 225004
[10] Suttrop W *et al* 2011 *Plasma Phys. Control. Fusion* **53** 124014
[11] Kirk A *et al* 2012 *Phys Rev Lett* **108** 255003
[12] Kirk A et al, 2013 *Nucl. Fusion* **53** 043007
[13] Kirk A *et al Plasma Physics and Controlled Fusion* **55** 015006 (2013)
[14] Liang Y *et al* 2010 *Nucl Fusion* **50** 025013
[15] Liang Y *et al* 2013 *Nucl Fusion* **53** 073036
[16] Saarelma S *et al* 2011 *Plasma Phys. Control. Fusion* **53** 085009
[17] Snyder PB *et al* 2007 *Nucl. Fusion* **47** 961
[18] Osborne TH *et al* 2008 *Journal of Physics: Conference Series* **123** 012014
[19] Chapman IT *et al* 2012 *Nuclear Fusion* **52** 123006
[20] Chapman IT *et al* 2013 *Phys Plasmas* **20** 056101

[21] Lao L *et al* 2005 *Proc. 47th Annual Meeting of Division of Plasma Physics (AIP)* CP1.00034
[22] R. Fischer *et al.* "Effect of non-axisymmetric magnetic perturbations on profiles at ASDEX Upgrade", 2011 *38th EPS Conference on Plasma Physics (Strasbourg)* P1.072 (http://ocs.ciemat.es/EPS2011PAP/pdf/P1.072.pdf)
[23] R Fischer et al, 2012, *Plasma Phys. Control. Fusion* **54** 115008
[24] J. C. Fuchs *et al.* "Influence of non-axisymmetric magnetic perturbations on the equilibrium reconstruction at ASDEX Upgrade", 2011 *38th EPS Conference on Plasma Physics (Strasbourg)* P1.090 (http://ocs.ciemat.es/EPS2011PAP/pdf/P1.090.pdf)
[25] Chapman IT *et al* 2007 *Nucl Fusion* **47** L36
[26] IT Chapman et al, 2012 *Plasma Phys Control Fusion* **54** 105013
[27] Lanctot MJ *et al* 2011 *Phys Plasmas* **18** 056121
[28] Moyer, RA, et al. *Nuclear Fusion* **52** (2012) 123019
[29] Fundamenski W and Pitts R, *J. Nucl. Mater.* **319** 363 (2007)
[30] Kocan M, 2013 "Heat loads to the ITER first-wall panels in the ICRH-optimized plasma equilibrium" Tech. rep. ITER DML5YK
[31] JB Lister, A Portone and Y Gribov 2006 *Control Systems* **26** 79
[32] D Yadykin et al, *sub Plasma Phys Control Fusion* 2013 "Effect of the external helical fields on the plasma boundary shape in JET"
[33] L. Frassinetti et al, *Rev. Sci. Instrum.* **83** (2012) 013506
[34] Nardon E. 2007 Edge Localized modes control by resonant magnetic perturbations PhD Thesis Ecole Polytechnique http://www.imprimerie.polytechnique.fr/Theses/Files/Nardon.pdf
[35] JM Canik et al, *Nucl. Fusion* **52** 054004 (2012)
[36] TM Bird and CH Hegna, *Nuclear Fusion* **53** 013004 (2013)
[37] NM Ferraro et al, *Nucl Fusion* **53** 073042 (2013)
[38] M Becoulet et al, *24th IAEA Fusion Energy Conference, San Diego, USA* TH/2-1
[39] Ferraro NM, *Phys. Plasmas* **19** 056105 (2012)
[40] Spong DA et al, *Nucl Fusion* **41** 711 (2011)
[41] Lazerson SA et al, *39th EPS Conference on Plasma Physics, Stockholm, Sweden* 2012
[42] D Orlov et al. *Proc. 53rd Annual Meeting of Division of Plasma Physics (AIP)* Poster GP8.77 (2012)
[43] GTA Huysmans et al, *Plasma Phys Control Fusion* **51** 124012 (2009)
[44] Evans T *et al* 2005 *J Phys: Conf Ser* **7** 174
[45] Wingen A *et al* 2009 *Nucl Fusion* **49** 055027
[46] Jakubowski MW *et al* 2009 *Nucl. Fusion* **49** 095013
[47] Nardon E *et al* 2011 *J. Nucl. Materials* **415** S914
[48] Cahyna P *et al* 2011 *J. Nucl. Materials* **415** S927
[49] Schmitz O *et al* 2008 *Plasma Phys Control Fusion* **50** 124029
[50] Casper T et al, 2012 *24th IAEA Fusion Energy Conference, San Diego, USA* ITR/P1-15
[51] Gribov Y and Loarte A 2012 "Curents in ELM coils for edge plasma shape perturbation studies" Tech. rep. ITER 98BA5X
[52] S Saarelma et al, *Nuclear Fusion* **52** 103020 (2012)
[53] Lazerson SA and Chapman IT *Plasma Phys Control Fusion* **55** 084004 (2013)
[54] Orain F *et al* 2013 *sub Phys Plasmas* "Nonlinear MHD modelling of the pasma response to resonant magnetic perturbations"
[55] Harrison JR *et al* 2013 *sub Nuclear Fusion* "Characteristics of X-point Lobe Structures in Single-Null Discharges on MAST"

The Princeton Plasma Physics Laboratory is operated
by Princeton University under contract
with the U.S. Department of Energy.

Information Services
Princeton Plasma Physics Laboratory
P.O. Box 451
Princeton, NJ 08543

Phone: 609-243-2245
Fax: 609-243-2751
e-mail: pppl_info@pppl.gov
Internet Address: http://www.pppl.gov